

Probing Neural Networks for Dynamic Switches of Communication Pathways

Holger Finger^{1,2,*†}, Richard Gast^{2,3,†}, Christian Gerloff⁴, Andreas K. Engel¹, Peter König^{1,2}

*For correspondence:
holger.finger@uos.de (HF)

†These authors contributed equally to this work

¹Department of Neurophysiology and Pathophysiology, University Medical Center Hamburg-Eppendorf, Hamburg; ²Institute of Cognitive Science, University of Osnabrück, Osnabrück; ³MPI for Human Cognitive and Brain Sciences, Leipzig; ⁴Department of Neurology, University Medical Center Hamburg-Eppendorf, Hamburg

Abstract Dynamic communication and routing play important roles in the human brain to facilitate flexibility in task solving and thought processes. Here, we present a network perturbation methodology that allows to investigate dynamic switching between different network pathways based on phase offsets between two external oscillatory drivers. We apply this method in a computational model of the human connectome with delay-coupled neural masses. To analyze dynamic switching of pathways, we define four new metrics that measure dynamic network response properties for pairs of stimulated nodes. Evaluating these metrics for all network pathways, we found a broad spectrum of pathways with distinct dynamic properties and switching behaviors. Specifically, we found that 60.1% of node pairs can switch their communication from one pathway to another depending on their phase offsets. This indicates that phase offsets and coupling delays play an important computational role for the dynamic switching between communication pathways in the brain.

Introduction

Over the past decades it has been shown that the brain, facing a specific task or not, reveals a well-structured functional organization (*Damoiseaux et al., 2006; Van Den Heuvel and Pol, 2010; Cabral et al., 2017*). This has been specifically investigated for resting-state networks (*Mantini et al., 2007; Brookes et al., 2011; Calhoun et al., 2008; Deco et al., 2017*), but also for other networks when the brain is performing different tasks (*Greicius et al., 2003; Calhoun et al., 2008*). These findings lead to the idea that resting-state networks describe an inherent functional organization of the brain which is optimized to perform a wide range of tasks it encounters frequently (*Fox et al., 2005; Engel et al., 2013*). If faced with a task that requires synchronization between brain areas not typically coupled at rest, this organization has to be altered temporarily in order to perform that task efficiently (*Gross et al., 2004; Raichle, 2015*).

Within a complex network like the human brain, multiple structural pathways exist between most pairs of nodes given a sufficiently high spatial resolution. Since synchronization along such pathways seems to play an important role in the formation of functional clusters, we set out to identify general principles of how these pathways interact with each other during synchronization processes. Several studies have emphasized the importance of information transmission delay for synchronization processes as well as its role in the formation of functional clusters in the

Box 1. Significance

A big challenge in elucidating information processing in the brain is to understand the neural mechanisms that dynamically organize the communication between different brain regions in a flexible and task-dependent manner. In this theoretical study, we present an approach to investigate the routing and gating of information flow along different pathways from one region to another. We show that stimulation of the brain at two sites with different frequencies and oscillatory phases can reveal the underlying effective connectivity. This yields new insights into the underlying processes that govern dynamic switches in the communication pathways between remote sites of the brain.

brain (*Engel et al., 1992; Deco and Corbetta, 2011; Deco et al., 2011; Cabral et al., 2011; Siegel et al., 2012; Fries, 2015; Finger et al., 2016; Cabral et al., 2017*). Thus, we hypothesize the time lag inherent to a communication path to be a key factor in the interaction between multiple pathways. These time windows are determined by axonal signal transmission delays as well as rise and decay properties of the post-synaptic response. Here, we focus on the former, expecting region-specific differences in the latter to be negligible for the long-range connections considered in this study. In particular, we predict that two brain regions trying to communicate at a certain frequency with a given phase offset will use only a fraction of their available communication paths. Further, we predict that the selection of communication paths will be influenced by their interaction time windows.

To test these hypotheses, we approximate cortico-cortical communication processes via a computational network model of delay-coupled, oscillating nodes. We introduce an extrinsic stimulation set-up for this model that allows to detect network interactions between pairs of nodes. This stimulation approach relies on the entrainment of a given pair of nodes to oscillate at the same frequency, but with a certain phase lag relative to each other. Comparing the coherence along different pathways over different stimulation phase offsets then reveals the phase preferences for different routes. While Figure 1A illustrates the extrinsic stimulation setup, Figure 1B motivates the use of different stimulation phase lags. It is important to note that even in the absence of any interaction through the network, there might be some induced trivial coherence between two stimulated nodes due to the external signal (Figure 1B). Thus, the coherence is measured for many different stimulation phase offsets and the measurement with the lowest coherence is chosen as the baseline. Any deviation in the coherence from this baseline can be attributed to induced changes in the coupling between the two stimulated nodes through the network, which may happen due to a switching in the pathways (compare Figure 1C and 1D). We propose that these differences in phase preferences at different pathways act as a switching and gating mechanism used by the brain to establish communication between remote brain areas when needed. Our method allows to investigate these mechanisms by probing the network for these dynamic switches in communication pathways.

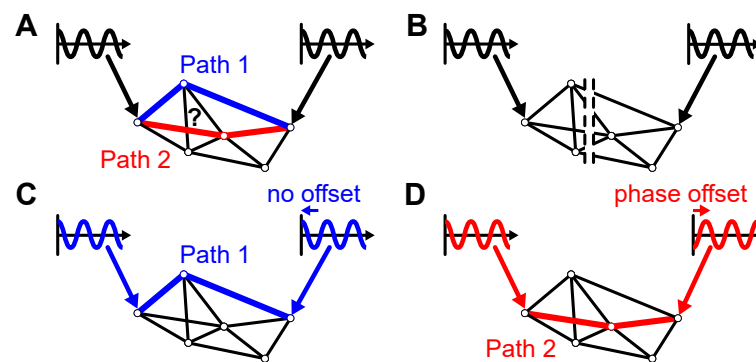


Figure 1. Illustration of the stimulation methodology and different possible outcomes. (A) The stimulation at the two nodes could potentially activate different paths (blue or red) in the network. (B) As an alternative explanation it could also be possible that a coherence between the two nodes is induced even in the absence of any direct interaction in the network. (C) In this example a stimulation phase offset of 0π induces a network interaction between the two stimulated nodes through path 1 (blue). (D) In contrast, when stimulating with a phase offset of π another path is activated (red).

Results

We first present results of simulations in simple networks of only 2 or 3 nodes. Specifically, we show how the coherence between a pair of stimulated nodes depends on the transmission delay of their connections and on the relative phase offsets between the two stimulation signals. Subsequently, we move on to a model of the cortico-cortical synchronization processes within a single hemisphere of the human brain. Cortico-cortical coupling strengths and delays were informed by an approximation of the human connectome obtained from diffusion tensor imaging (DTI) data. Additionally, we fit the model to match functional connectivities calculated from electroencephalography (EEG) recordings. In this model, we show how the coherence between stimulated nodes changes over phase lags and how this effect relates to the connectedness and distance of the nodes. In a final step, we identify the pathways responsible for the interaction between the stimulated nodes, analyze their phase lag preferences and identify cases of phase-related switching between pathways. For all simulations, we used the computational model defined in Box 2.

Simple Models With 2 or 3 Nodes

The idea behind the extrinsic stimulation approach can be well explained using a simple toy-model of 2 directly coupled Jansen-Rit nodes, where each node is stimulated with a $f_{\text{ext}} = 11$ Hz sinusoidal signal with strength $c_{\text{ext}} = 0.25$ mV. Figure 2 shows the coherence between the driven nodes for systematic changes in the phase offset between the stimuli and the distance between the coupled nodes. While uni-directionally coupled nodes can have preferences for any stimulation phase offset, as shown in Figure 2A, bi-directionally coupled nodes are more susceptible for stimulation at in- or anti-phase (see Figure 2B). This shows that the communication between coupled pairs of nodes can be modulated by stimulation and that communication channels can have characteristic stimulation phase offset preferences, depending on their length (König and Schillen, 1991).

To quantify the modulation of communication, we define the pathway-synchronization-facilitation (PSF), measuring for a given pair of weakly stimulated network nodes k_i and k_j how their interaction is dependent on specific phase offsets:

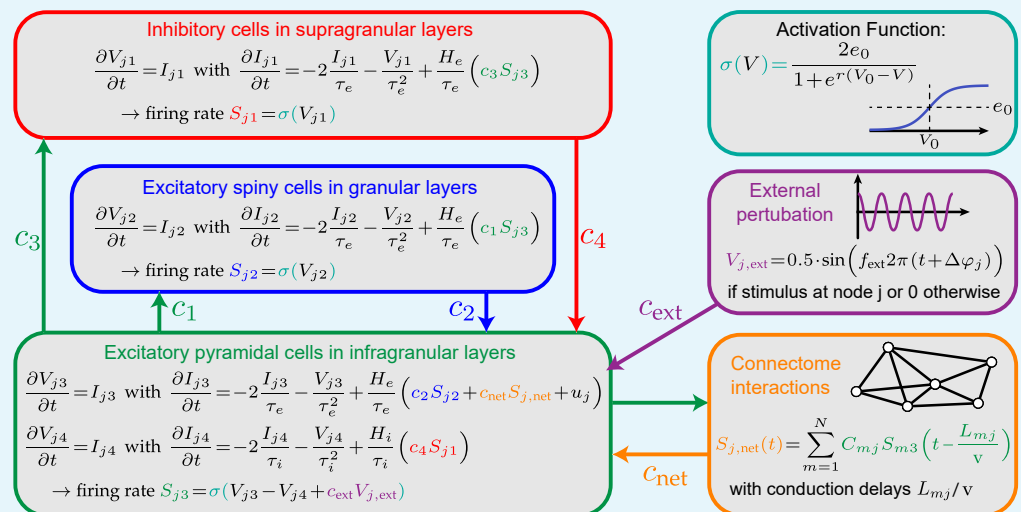
$$\text{PSF}(k_i, k_j) = \max_{0 \leq \Delta\varphi \leq 2\pi} \left(\text{coh}(k_i, k_j, \Delta\varphi) \right) - \min_{0 \leq \Delta\varphi \leq 2\pi} \left(\text{coh}(k_i, k_j, \Delta\varphi) \right),$$

where $\text{coh}(k_i, k_j, \Delta\varphi)$ is the coherence between network nodes k_i and k_j for stimulation phase offset $\Delta\varphi$. The PSF is high for node pairs if their coherence is high for one stimulation phase offset and

Box 2. Computational Model

Our computational model is based on the widely used Jansen-Rit neural mass model (Jansen and Rit, 1995) which employs a mean-field approach to model the interaction between cell populations in the infragranular (depicted in green), granular (depicted in blue), and supragranular (depicted in red) layer, as illustrated with the relevant equations in the Figure. The function $\sigma(V)$ that transforms average membrane potentials to firing rates is a parameterized sigmoid (depicted in cyan). The standard parametrization originally proposed by Jansen and Rit reflects cortical oscillatory activity in the alpha frequency band. These parameters were chosen based on experimental findings in the neuroscience literature and are reported in Table 2 in the Methods and Materials section. Since the purpose of this article is the investigation of the effect of pathway time-scales on neural synchronization processes and not the effect of node time-scales, we decided to use this standard parametrization for each node in our network (Jansen and Rit, 1995).

For the purpose of investigating networks of extrinsically perturbed Jansen-Rit models, the following two extensions were added: First, we coupled multiple Jansen-Rit nodes via delayed, weighted connections between their infragranular pyramidal cell populations (depicted in yellow). Secondly, weak external drivers were applied at two stimulation sites influencing the average membrane potential of the infragranular layer with phase offset $\Delta\varphi$ between the two drivers (depicted in purple).



Box 2 Figure 1. Neural mass model with external stimulation. A schematic of the neural mass model showing the interactions between the three neuronal populations in the infragranular, granular, and supragranular layer. Each post-synaptic potential is modeled using two differential equations (average membrane potentials V and average synaptic currents I). Several of these neural mass models are interacting through a connectivity matrix (yellow). The external perturbation (purple) modulates the average membrane potential of pyramidal cells at 2 nodes in the network.

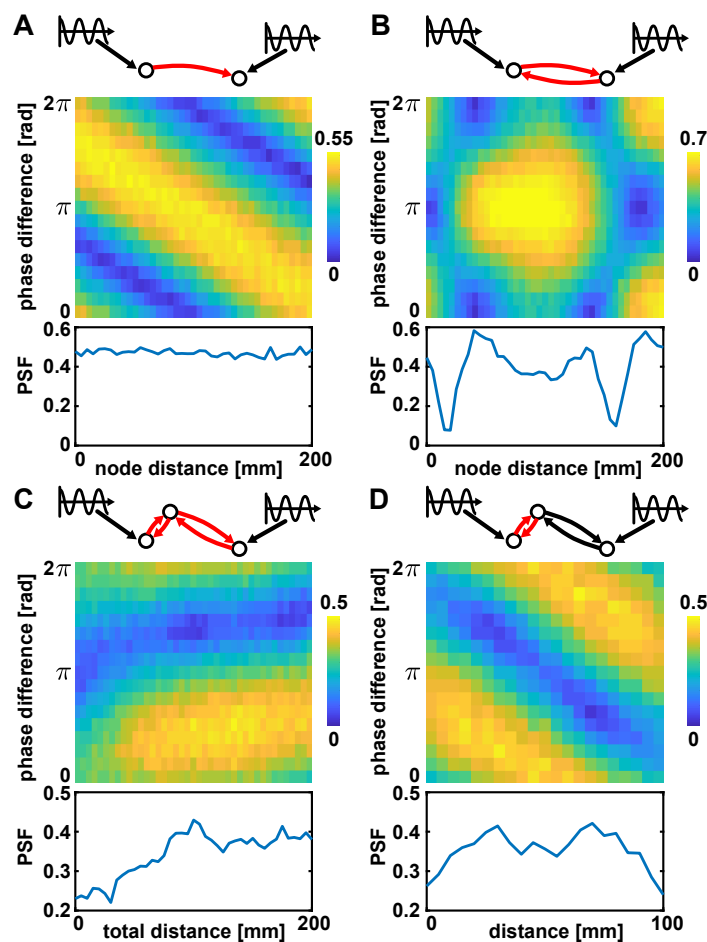


Figure 2. Simulations with 2 or 3 nodes, where the red edges correspond to the distance that was varied. Color indicates the coherence between the two driven nodes. The PSF values are shown at the bottom of each panel. (A) Nodes with direct uni-directional coupling. (B) Nodes with direct bi-directional coupling. (C) Nodes with indirect (via a third node) bi-directional couplings. The intermediate node was placed at 25 % of the total connection distance, while the overall distance between the outer nodes was varied. (D) Nodes with indirect bi-directional couplings where the overall distance was kept at 100 mm, while the intermediate node was positioned at varying positions along the connection. Parameters used in all panels: $v = 3$ m/s, $C_{mj} \cdot c_{\text{net}} = 0.1$ if there is a connection from node m to j or 0 otherwise.

low for another, i.e., the relative phase of the stimulation at the two sites matters strongly. The PSF curves in Figure 2A and 2B show that in both cases there is a PSF effect ($\text{PSF} > 0$) and in the case of bi-directionally coupled nodes the strength of this effect depends on the distance between the nodes.

To extend this idea to communication via indirect pathways, we investigated synchronization between 2 nodes connected only indirectly via a third intermediate node. We used bi-directional couplings for both connections and both end nodes were stimulated as described previously. As can be seen in Figure 2C and 2D, the interaction between the two weakly stimulated nodes not only depended on the length of the connection, but potentially also on the relative position of the third node on the indirect path.

Connectome Model Without Stimulation

As shown in the previous section, the coherence in a network of only three nodes can already exhibit very complex dependencies on the stimulation phase offset. Next, we wanted to analyze network communication patterns in the case of a complex network with multiple competing pathways.

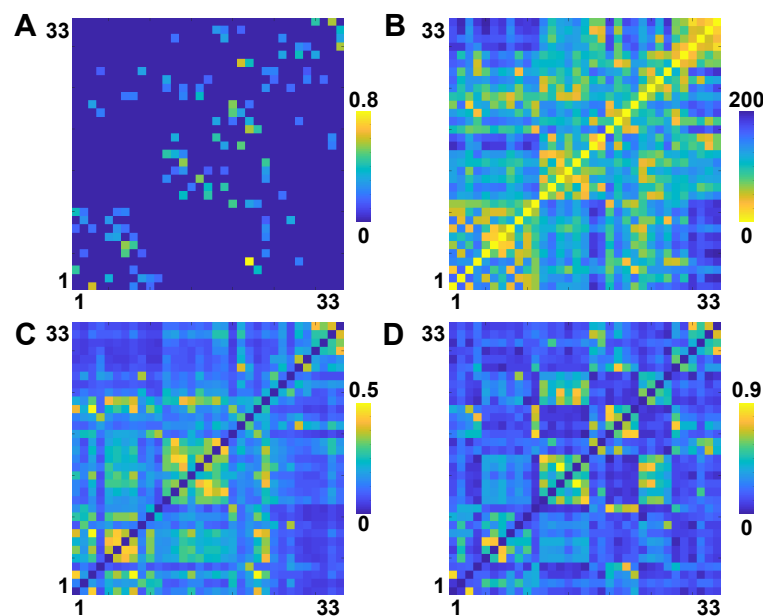


Figure 3. Pairwise measures of connectivity and distance between all 33x33 region pairs. (A) Structural connectivity matrix with all connections smaller 0.1 set to 0. (B) Inter-regional distances in mm. (C) Functional connectivity matrix derived from coherence of EEG data bandpass-filtered around 10 Hz. (D) Functional connectivity derived from coherence of neural mass model simulations bandpass-filtered around 10 Hz.

To this end, we used a model of 33 delay-connected nodes, representing one hemisphere of the human connectome (Finger et al., 2016). The structural connectivity matrix was obtained from DTI-based tractography data as described in more detail in the Methods and Materials section. Figure 3A shows the sparse connectivity matrix C_{mj} used to connect the 33 regions and Figure 3B the corresponding distances L_{mj} between region pairs. These two matrices are used for connecting the different populations of excitatory pyramidal cells (green in Box 2) in a delay-coupled network of a single-hemisphere.

For the same 33 regions, EEG resting-state recordings from the same subjects were used to calculate pairwise coherences in the 10 Hz range as shown in Figure 3C. Similarly, we simulated the 33 connected neural-mass-models and processed the time-series of the pyramidal cells in the same way as the EEG data. This yielded a 33 x 33 functional connectivity matrix which we compared to the empirical functional connectivity by calculating the Pearson correlation coefficient.

The selection of parameters was based on the rationale to match the functional connectivity observed in the network model as good as possible to empirical EEG-based functional connectivity from human subjects. We performed a grid search over global structural connectivity scaling c_{net} and transmission velocity v to obtain the best match between modeled and empirical data. By fitting the velocity, we ensured that our pathway delays reflect realistic, empirically observed timescales of cortico-cortical interactions. We found the highest correlation ($r = 0.57$) for $c_{net} = 20$ and $v = 3$ m/s, so that we used these parameters for subsequent analyses (Figure 3D). Notice that this correlation is comparable with values of other bottom-up models reported in the literature (Messé et al., 2015; Finger et al., 2016), which is remarkable considering that we set a substantial amount of structural connections to 0. Interestingly, both simulated and empirical functional connectivity correlate stronger with the inter-regional fiber distances ($r_{sim} = -0.65$, $r_{emp} = -0.70$) than with the structural connectivity ($r_{sim} = 0.65$, $r_{emp} = 0.51$), highlighting the importance of signal transmission delays for cortical coupling processes.

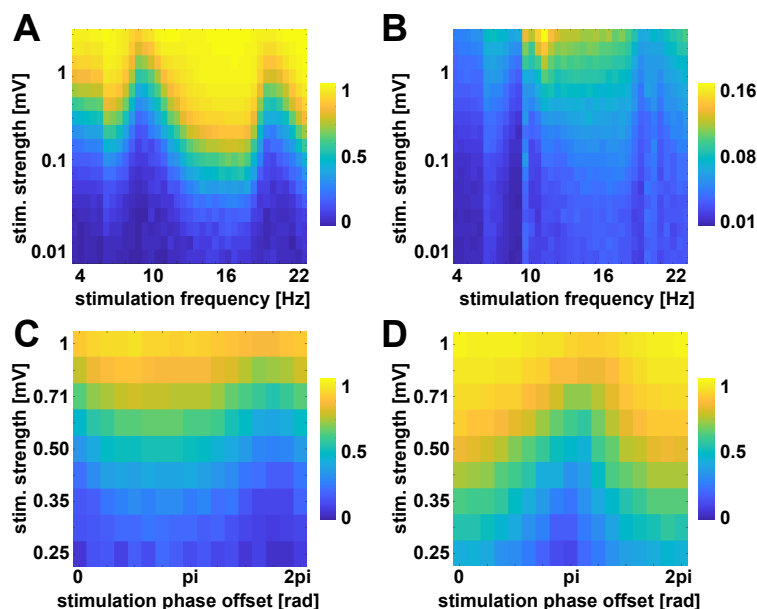


Figure 4. Stimulation parameter evaluation. (A) Coherence between the stimulus and the stimulated region for varying stimulus strength and frequency. The color corresponds to a mean value over 5 simulations at randomly chosen network nodes. (B) Coherence between the stimulus and the full network averaged over all 33 nodes for varying stimulus strength and frequency. The coherence was calculated between the stimulus and each region and then averaged. (C and D) Coherence between two stimulated nodes for varying stimulation strength and phase offset. C and D correspond to two different node pairs that were stimulated demonstrating the variability in phase lag preferences expressed by different pairs.

Connectome Model With Stimulation

Based on this model of cortical activity we used the stimulation approach to investigate how pathways facilitate synchronization between network nodes at certain phase lags between the nodes. Specifically, we weakly stimulated different pairs of cortical regions with varying phase offsets between the two stimulation signals while measuring the coherence between the stimulated nodes at each phase offset. As argued above, finding differences in the coherence over stimulation phase offsets would indicate phase-specific communication modulation between the stimulated nodes. Before analyzing PSF effects in the connectome model, it was necessary to determine the optimal stimulation frequency and strength for this model. This was performed in two steps. First, we stimulated a single region in our network with a stimulus of varying frequency (4-22 Hz) and strength (0.01-2 mV) while evaluating the coherence between region and stimulus. The mean coherence (mean over 5 different stimulated nodes) for each parameter combination can be observed in Figure 4A. They reflect the well-studied relationship between a driver and an oscillator described by the so-called Arnold tongue (Boyland, 1986). Since our main analysis will focus on coupling effects through different network paths between two stimulated nodes, we also calculated the coherence between stimulus and all network nodes (Figure 4B). This average coherence to the full network was strongest at 9-11 Hz, which is also the intrinsic frequency of unperturbed network nodes (Schmidt et al., 2014). Interestingly, at this frequency the coherence to the directly stimulated node was weakest (compare Figure 4A). Based on this, we set the frequency of our stimulus to 11 Hz, at which the network (and not only the directly stimulated node) was most susceptible for entrainment by an external stimulation.

In a second step, we stimulated pairs of nodes with 11 Hz stimuli. We varied the stimulus strength (0.25 - 1 mV) and the relative phase offset between the stimuli ($0 - 2\pi$), while evaluating the coherence between the stimulated nodes. All other parameters were chosen to be the same as for the previous simulation. As can be seen in Figure 4C and Figure 4D, the variance of the

Table 1. Model Parameters

Param.	Value	Interpretation
c_{net}	20	global connection strength scaling
v	3 m/s	global velocity scaling
f_{ext}	11 Hz	extrinsic stimulation frequency
c_{ext}	500 μV	amplitude of extrinsic stimuli

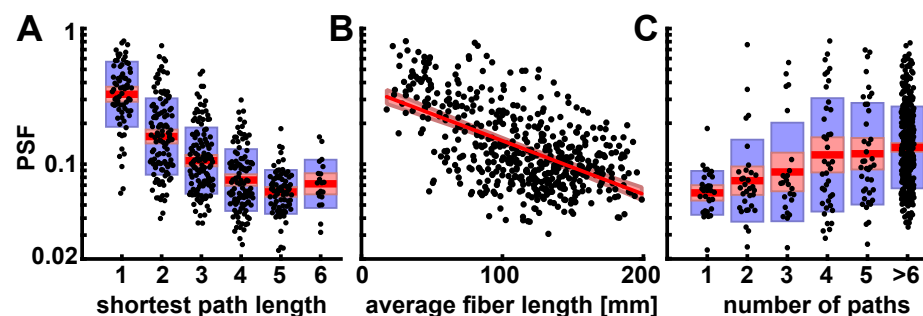


Figure 5. Pathway Synchronization Facilitation (PSF). All panels show the PSF on a logarithmic vertical axis and red areas indicate 95 % confidence intervals. Blue boxes indicate 1 standard deviation. (A) Dependence of PSF effect on shortest path length between the node pairs. (B) Correlation between PSF effect and average fiber length along the shortest pathway between the stimulated nodes. (C) Dependence of the PSF effect on the number of paths connecting the stimulated nodes.

coherence over phase offsets depended on the stimulation strength. Based on visual inspection of the coherence patterns of 20 different region pairs, we chose our stimulus scaling to be $c_{\text{ext}} = 0.5$ mV, leaving the variance of the post-synaptic potential of the neural masses in a biologically plausible range and such that the external driver is relatively weak in comparison to the internal network dynamics. This gave us the final set of global model parameters which were used throughout all subsequent simulations and are reported in Table 1.

The variability in the coherence between stimulated region pairs that we observed not only over stimulation phase offsets but also over different pairs (as depicted for 2 exemplary region pairs in Figure 4C and 4D) shows that the stimulated region pairs interacted with each other and that the interactions showed a characteristic profile of phase offset preferences. To statistically confirm the variance in the coherence between stimulated region pairs over phase offsets, we ran simulations with stimulations of each possible node pair. Again, we varied the phase offset between the two stimuli (16 equally spaced phase offsets between 0 and 2π) and evaluated the coherence between the stimulated nodes for each phase offset. Subsequently, those coherences were used to calculate the PSF for each region pair as defined in equation ???. Using a one-sample t-test, we found the PSF effect to be significantly larger than zero (mean = 0.1567, CI = [0.1445, 0.1689], $t = 25.2595$, $p < 0.0001$). Hence, we were able to show with our extrinsic stimulation approach that pathways facilitated synchronization between cortical nodes and that the facilitatory strength depended on the phase lag between the region's average PSPs.

With the PSF effect established, we continued by investigating its dependence on certain features of the underlying structural connectivity graph. For this purpose, we searched for all possible pathways between each pair of stimulated nodes based on the structural connectivity matrix reported in Figure 3A. Since every stimulated pair of nodes was connected by at least one path via at most 6 edges, we restricted the search to pathways including 6 edges at maximum. With these pathways at hand, we started out by evaluating how the PSF effect changed with increasing network distance. An analysis of variance showed that the effect of shortest path length (minimum number of edges separating a pair) on $\log(\text{PSF})$ was significant, $F(5, 521) = 97.6141$, $p < .0001$. As

can be seen in Figure 5A, we observed the trend that the PSF effect decreases with the number of nodes separating the stimulated nodes. Furthermore, as depicted in Figure 5B, this trend was supported by a significant correlation between the PSF effect and the length of the shortest pathway between the stimulated nodes ($r = -0.56$, $p < .0001$), a measurement that is strongly related to both interregional distance and minimal number of separating edges. Thus, we conclude that there is a tendency for a decrease in the interaction of stimulated node pairs with increasing network distance between the nodes, where network distance can be measured either as the number of edges or as the summed up length of the edges of the shortest pathway connecting the nodes.

Next, we investigated the dependence of the PSF effect on the connectedness between the stimulated nodes. An analysis of variance showed that the effect of the number of connecting paths (only counting paths with 5 edges or less, all nodes with more than 5 connecting paths were pooled into one level) on $\log(\text{PSF})$ was significant, $F(5,501) = 10.0827$, $p < .0001$. The latter result can be observed in detail in Figure 5C.

Evaluation of Pathway Activation

Having described the influence of the external driver on the coherence between stimulated nodes, we next identified which particular pathways were involved in this interaction. For this analysis, we define the pathway activation (PA) for a pathway through n nodes k_i with $i = 1..n$ at a phase offset $\Delta\phi$ as the minimum of the pairwise coherences between neighboring pathway nodes:

$$PA(k_1..k_n, \Delta\phi) = \min_{i=1..n-1} \left(\text{coh}(k_i, k_{i+1}, \Delta\phi) \right).$$

In other words, if communication fails at any point along a pathway, leading to a reduced coherence between the involved nodes, this is considered to be a bottleneck for the information flowing through that pathway. We evaluated the pathway activation (PA) for all pathways of up to $n = 5$ nodes connecting a given pair of stimulated nodes for all stimulation phase offsets. Doing this for each stimulated node pair, we found different classes of pathway interactions: Some pairs show only a very small selectivity for the stimulation phase offset (Figure 6A), while other node pairs were connected by paths with PA values with a strong dependence on the phase offset (Figure 6B, 6C). Moreover, some of these node pairs switched their interaction between different pathways depending on the stimulation phase offset, as shown in Figure 6C and the two switching pathways in Figure 6D and 6E.

To further analyze how the communication via specific pathways depends on the stimulation phase offset, we define the pathway phase selectivity (PPS) of a pathway P_1 similar to the PSF as

$$PPS(P_1) = \max_{\Delta\phi} (PA(P_1, \Delta\phi)) - \min_{\Delta\phi} (PA(P_1, \Delta\phi)),$$

Pathways with relatively constant PA values for all stimulation phase offsets have a low PPS (example in Figure 6A), while pathways with a high variation in the PA values have a high PPS (example in Figure 6B and 6C). The evaluation of PPS values for all node pairs results in a bimodal distribution (Figure 6F). The activation of pathways in the first mode at $PPS = 0.1$ is very hard to influence with phase offsets. But we also found many node pairs with pathways in the second mode at $PPS = 0.35$. The communication of these later node pairs can be modulated using different phase offsets.

In a next step, we analyzed the relationship of pathway-specific phase preferences (as shown in Figure 6A-C) to the phase preferences of the stimulated nodes (as shown in Figure 4C-D). We chose the most active pathway per node pair (averaged over all stimulation phase offsets) and calculated the phase difference between the stimulation phase offset with the highest coherence and the stimulation phase offset with the highest PA. The histogram of these phase differences is significantly different from uniform, $\chi^2(15, N = 514) = 273.05$, $p < .001$, and has a peak at 0 (Figure 6G). In contrast, a similar analysis for the second strongest pathway (excluding all pathways with overlapping sections with the strongest path), results in a histogram that does not differ from a uniform distribution, $\chi^2(15, N = 514) = 14.06$, $p = 0.52$ (Figure 6H). Therefore, we conclude that the

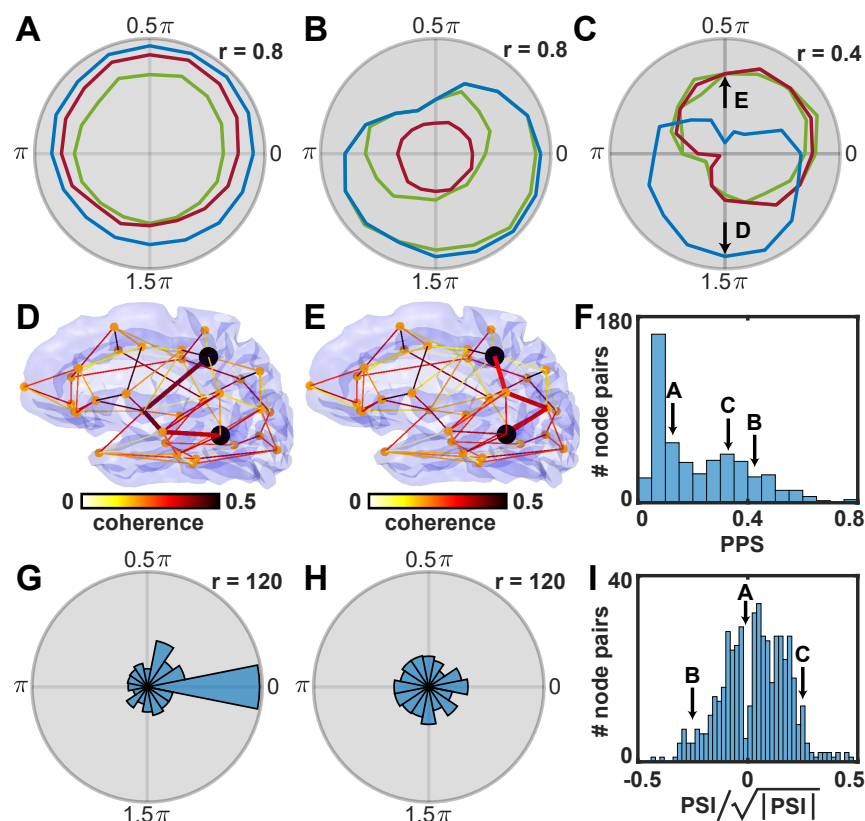


Figure 6. Dependence of path activation (PA) on stimulation phase offset. Panels (A-C) show the PA values (radius) for different stimulation phase offsets (angle) for exemplary node pairs. Blue corresponds to the pathway with the strongest overall PA. Red corresponds to the second strongest pathway that has no overlapping segments with the strongest. Green curves show the strongest of the remaining pathways (with possible overlapping path segments with the former two). The two arrows in (C) indicate the phase offsets which are used in panels (D-E). (D) Connectome pathways for stimulation of the node pair shown in (C) at phase offset 1.5π . The two stimulated nodes are shown as two black dots. The most active pathway at this stimulation phase offset is highlighted with a stronger line width. All colors correspond to the coherence of nearest neighbours in the connection graph. (E) Similar to (D) but for stimulation phase offset 0.5π with a different most active pathway. (F) Histogram of pathway phase selectivity. The values of the strongest paths of examples shown in (A-C) are marked with arrows. (G) Histogram of phase differences between the stimulation phase offset where the most active pathway has the highest pathway activation and the stimulation phase offset where the coherence between the stimulated nodes was highest. (H) Similar to (G) but for the second most active pathway (excluding path overlaps with the most active pathway). (I) Histogram of normalized pathway switching index between the strongest and second strongest pathways. The values of the node pairs of examples shown in (A-C) are marked with arrows. The square-root normalization of the PSI transforms back from the space of multiplied coherence values to the original non-squared coherence space (analogous to a transformation from variance to standard-deviation).

270 pathway with the strongest PA shows a similar phase preference as the coherence between the two
271 stimulated nodes.

272 Finally, we quantified the switching between the strongest and second strongest pathway per
273 node pair. To this end, we define the pathway switching index (PSI) between pathways P_1 and P_2 as

$$\text{PSI}(P_1, P_2) = \max_{\Delta\varphi} (\text{PA}(P_1, \Delta\varphi) - \text{PA}(P_2, \Delta\varphi)) \\ \cdot \max_{\Delta\varphi} (\text{PA}(P_2, \Delta\varphi) - \text{PA}(P_1, \Delta\varphi)),$$

274 The PSI is positive if the two pathways switch their activation depending on the stimulation phase
275 offset, meaning that at one phase offset the first path is more active and at another phase offset
276 the second path is more active. We found that 60.1% (309 of 514) of node pairs have a positive
277 PSI between their non-overlapping strongest and second strongest pathways (Figure 6I). These
278 results suggest that in this network of 33 nodes of the human connectome many node pairs have
279 the capacity to switch their communication between at least two different pathways with a PA
280 characteristic similar to the example shown in Figure 6C.

281 Discussion

282 We have carried out a computational study of cortico-cortical synchronization processes that
283 strongly emphasizes the role of phase relationships for dynamic switches in communication path-
284 ways. In this process, we introduced a novel method to detect network interactions between pairs
285 of cortical regions via an extrinsic stimulation scheme. Using our method, we were able to quantify
286 the influence of different pathways on cortico-cortical synchronization processes between all pairs
287 of 33 brain regions and could further identify the pathways those region pairs use to interact with
288 each other. These pathways represent communication channels with distinct interaction time
289 windows.

290 One of the main findings of our work is that we found the ability of regions to communicate via
291 these channels to depend on the phase lag at which they try to synchronize. This finding is in line
292 with the communication-through-coherence theory that predicts neural communication to critically
293 depend on oscillatory phase differences and has received support from various experimental
294 results (*Fries, 2015*). In a transcranial magnetic stimulation study, *Elswijk et al.* demonstrated
295 the effect of the stimulation on primary motor cortex to depend on the oscillatory phase of the
296 latter (*Elswijk et al., 2010*). Similarly, *Helfrich et al.* found the performance in a visual detection
297 task to be modulated by the phase of a 10 Hz transcranial alternating current stimulation applied
298 to the parieto-occipital cortex. Together, these experimental results support the idea of the
299 communication-through-coherence theory that the effectiveness of neural communication between
300 a source and a target population is modulated by the oscillatory phase of the latter. In a study
301 using multielectrode recordings in frontal eye field and area V4 of monkeys, *Gregoriou et al.* were
302 able to show that neural populations at both recording sites synchronized at characteristic time
303 lags when processing a stimulus in their joint receptive field (*Gregoriou et al., 2009*). Based on
304 the communication-through-coherence theory this may be explained by the axonal and synaptic
305 delays of the communication channel between these two areas, which render synchronization at
306 this time lag most effective. The work presented in this article contributes to this line of arguing
307 via its systematic investigation of the dependence between communication channel delays and
308 neural synchronization. By finding that the synchronization of two brain regions via simultaneous
309 extrinsic stimulation has a preference for the phase relationship between the two stimulation
310 signals, we demonstrated the mechanistic role of phase lags for neural communication within a
311 computational model. We were able to extend this finding to single communication channels, i.e. we
312 showed that these channels can express more or less strong preferences for the phase lag between
313 the brain regions they connect. On the one hand, this emphasizes the potential importance of
314 communication channel delays for shaping the synchronization phase lag patterns of the brain. On

the other hand, it suggests the effectiveness of information exchange via a certain communication channel in the brain to depend on the phase relationship between the communicating sites.

The functional significance of these phase lag preferences is underlined by our finding that different communication channels may be employed at different stimulation phase offsets between the communicating regions. We believe that the switching between different synchronization phase lags could be an effective mechanism through which brain regions can dynamically change their communication channels. Both external stimuli and network intrinsic signals could act as phase-resetting mechanisms at the communicating sites and thus switch from one communication channel to another within a few oscillatory cycles (Canavier, 2015). As suggested in (Engel and Singer, 2001; Engel et al., 2013), such a mechanism would provide the necessary flexibility to allow for the dynamic binding of remote neural representations into different combined representations.

Taken together, our results suggest a potential mechanism the human brain might have developed to use the physiological constraints imposed by coupling delays to its computational advantage. They motivate future brain stimulation studies to investigate phase-lagged neural synchronization, e.g., through multi-site transcranial stimulation, or optogenetics in combination with multielectrode recordings (Yazdan-Shahmorad et al., 2018). Thereby, the stimulation method we applied to our computational model could guide the development of brain stimulation protocols to probe dynamic switching between communication pathways in the brain. Additionally, our stimulation method and graph metrics are applicable in future theoretical studies characterizing the dynamic properties of network graphs.

Methods and Materials

In the following, we present the detailed parameters of the neural mass model, the preprocessing of the structural connectivity, and the functional connectivity.

Neural Mass Model

All simulation results reported refer to 16 minutes of simulated network behavior, using an explicit Euler method with an integration step-size of 0.5 ms. The parameters of the neural mass model are shown in Table 2.

Table 2. Model Parameters

Param.	Value	Interpretation
H_e	3.25 mV	avg. gain of excitatory synapses
H_i	22 mV	avg. gain of inhibitory synapses
τ_e	10 ms	lumped time constant of excitatory synapses
τ_i	20 ms	lumped time constant of inhibitory synapses
c_1	135	avg. number of contacts from pyramidal cells to exc. interneurons
c_2	$0.8 \cdot c_1$	avg. number of contacts from exc. interneurons to pyramidal cells
c_3	$0.25 \cdot c_1$	avg. number of contacts from pyramidal cells to inh. interneurons
c_4	$0.25 \cdot c_1$	avg. number of contacts from inh. interneurons to pyramidal cells
e_0	2.5 Hz	maximum scaling of the synaptic gain
r	0.56 mV^{-1}	steepness of the sigmoid function
V_0	6 mV	value with 50% of max. firing rate
u_j	120 - 320 Hz	sub-cortical noise distributed uniformly

In the Jansen-Rit model, signal transmission between cell populations is realized via a convolution of average pre-synaptic firing rates with a post-synaptic response kernel. These convolution operations are mathematically described by the coupled ordinary differential equations in Box 2 (each line describes a synaptic convolution operation) and turn pre-synaptic firing rates into post-synaptic potentials. The simple exponential form of the response kernel is in line with empirically

measured post-synaptic responses *Gerstner et al. (2014)* and provides a sufficient approximation of synaptic response time scales for our purposes. To translate post-synaptic responses back into firing rates, an instantaneous sigmoidal transform is used as shown in Box 2.

Structural Connectivity and Distance Estimates

In a first step to building a bottom-up model of cortical activity we needed to approximate the structural connections between different brain regions. As mentioned in the introduction, this can be done via DTI recordings. However, there are several technical limitations as to what extend human SC can be approximated based on DTI, one of them being the systematic underestimation of inter-hemispheric connections (*Li et al., 2012; Wedeen et al., 2008*). Thus we decided to restrict our analysis to the cerebral cortex of a single hemisphere. To this end, we used the same structural imaging data, pre-processing and probabilistic tracking pipeline as reported by Finger et al. (*Finger et al., 2016*), but restricted subsequent processing to the 33 regions of interest (ROIs) of the left hemisphere. This data set included diffusion- and T1-weighted images acquired from 17 healthy subjects (7 female, age mean = $65.6y \pm 10.9y$) with a 3 Tesla Siemens Skyra MRI scanner (Siemens, Erlangen, Germany) and a 32-channel head coil. The 33 ROIs were registered individually for each subject based on the 'Desikan-Killiany' cortical atlas available in the Freesurfer toolbox (surfer.nmr.mgh.harvard.edu) (*Desikan et al., 2006*). This gave us the euclidean distances between each pair of ROIs. The incoming connections to each region were normalized such that they summed up to 1. Since we were only interested in synchronization along indirect pathways, we needed some connections in our model to be strictly 0. Otherwise, it would be difficult to exclude potential synchronization along very weak direct connections. Hence, we chose to set all connections below a strength of 0.1 to zero. Afterwards, we re-normalized the input to each region such that they summed up to 1. The resulting SC matrix as well as the pair-wise distances are visualized in Figure 3A and 3B in the main paper.

Empirical Resting-State Functional Connectivity

Based on those SC and distance information we aimed to build a model of cortical activity able to reflect empirically observed synchronization behavior. Thus we needed empirical observations of cortical activity to evaluate our model. For this purpose, we acquired EEG data from the same 17 subjects as described above. This was done with 63 cephalic active surface electrodes arranged according to the 10/10 system (actiCAP R Brain Products GmbH, Gilching, Germany) for eight minutes of eyes-open resting-state. Again, data acquisition and pre-processing followed the same procedure as reported by Finger et al. (*Finger et al., 2016*). EEG time-series from the surface electrodes were projected onto the centers of the ROIs via a linear constraint minimum variance spatial beam former (*Van Veen et al., 1997*). The resulting source-space signals were band-pass filtered at 10 Hz and turned into analytic signals using the Hilbert transform. Subsequently, functional connectivity was evaluated as the coherence between all pairs of ROIs (*Andrew and Pfurtscheller, 1996*). This resulted in the 33 x 33 functional connectivity matrix that can be observed in Figure 3C in the main paper and served as optimization target for our model.

Acknowledgments

This research has been funded by the DFG (SFB 936, projects A2/A3/C1/Z1).

References

- Andrew C, Pfurtscheller G.** Event-related coherence as a tool for studying dynamic interaction of brain regions. *Electroencephalography and Clinical Neurophysiology*. 1996; 98(2):144–148.
- Boyland PL.** Bifurcations of circle maps: Arnol'd tongues, bistability and rotation intervals. *Communications in Mathematical Physics*. 1986; 106(3):353–381.

- 392 **Brookes MJ**, Hale JR, Zumer JM, Stevenson CM, Francis ST, Barnes GR, Owen JP, Morris PG, Nagarajan SS.
393 Measuring functional connectivity using MEG: methodology and comparison with fMRI. *NeuroImage*. 2011;
394 56(3):1082–1104.
- 395 **Cabral J**, Hugues E, Sporns O, Deco G. Role of local network oscillations in resting-state functional connectivity.
396 *NeuroImage*. 2011; 57(1):130–139.
- 397 **Cabral J**, Kringelbach ML, Deco G. Functional connectivity dynamically evolves on multiple time-scales over a
398 static structural connectome: Models and mechanisms. *NeuroImage*. 2017; .
- 399 **Calhoun VD**, Kiehl KA, Pearlson GD. Modulation of temporally coherent brain networks estimated using ICA at
400 rest and during cognitive tasks. *Human Brain Mapping*. 2008; 29(7):828–838.
- 401 **Canavier CC**. Phase-resetting as a tool of information transmission. *Current opinion in neurobiology*. 2015 Apr;
402 31:206–213. <https://www.ncbi.nlm.nih.gov/pmc/articles/PMC4375052/>, doi: 10.1016/j.conb.2014.12.003.
- 403 **Damoiseaux J**, Rombouts S, Barkhof F, Scheltens P, Stam C, Smith SM, Beckmann C. Consistent resting-state
404 networks across healthy subjects. *Proceedings of the National Academy of Sciences*. 2006; 103(37):13848–
405 13853.
- 406 **Deco G**, Corbetta M. The dynamical balance of the brain at rest. *The Neuroscientist*. 2011; 17(1):107–123.
- 407 **Deco G**, Jirsa VK, McIntosh AR. Emerging concepts for the dynamical organization of resting-state activity in the
408 brain. *Nature Reviews Neuroscience*. 2011; 12(1):43.
- 409 **Deco G**, Kringelbach ML, Jirsa VK, Ritter P. The dynamics of resting fluctuations in the brain: metastability and its
410 dynamical cortical core. *Scientific Reports*. 2017; 7(1):3095.
- 411 **Desikan RS**, Ségonne F, Fischl B, Quinn BT, Dickerson BC, Blacker D, Buckner RL, Dale AM, Maguire RP, Hyman
412 BT, et al. An automated labeling system for subdividing the human cerebral cortex on MRI scans into gyral
413 based regions of interest. *NeuroImage*. 2006; 31(3):968–980.
- 414 **Elswijk Gv**, Maji F, Schoffelen JM, Overeem S, Stegeman DF, Fries P. Corticospinal Beta-Band Synchronization
415 Entails Rhythmic Gain Modulation. *Journal of Neuroscience*. 2010 Mar; 30(12):4481–4488. [http://www.
416 jneurosci.org/content/30/12/4481](http://www.jneurosci.org/content/30/12/4481), doi: 10.1523/JNEUROSCI.2794-09.2010.
- 417 **Engel AK**, Gerloff C, Hlgetag CC, Nolte G. Intrinsic coupling modes: multiscale interactions in ongoing brain
418 activity. *Neuron*. 2013; 80(4):867–886.
- 419 **Engel AK**, König P, Kreiter AK, Schillen TB, Singer W. Temporal coding in the visual cortex: new vistas on
420 integration in the nervous system. *Trends in Neurosciences*. 1992; 15(6):218–226.
- 421 **Engel AK**, Singer W. Temporal binding and the neural correlates of sensory awareness. *Trends in Cognitive
422 Sciences*. 2001 Jan; 5(1):16–25. <http://www.sciencedirect.com/science/article/pii/S1364661300015680>, doi:
423 10.1016/S1364-6613(00)01568-0.
- 424 **Finger H**, Bönstrup M, Cheng B, Messé A, Hlgetag C, Thomalla G, Gerloff C, König P. Modeling of large-scale
425 functional brain networks based on structural connectivity from DTI: comparison with EEG derived phase
426 coupling networks and evaluation of alternative methods along the modeling path. *PLoS Computational
427 Biology*. 2016; 12(8):e1005025.
- 428 **Fox MD**, Snyder AZ, Vincent JL, Corbetta M, Van Essen DC, Raichle ME. The human brain is intrinsically organized
429 into dynamic, anticorrelated functional networks. *Proceedings of the National Academy of Sciences*. 2005;
430 102(27):9673–9678.
- 431 **Fries P**. Rhythms for Cognition: Communication through Coherence. *Neuron*. 2015 Oct; 88(1):220–235.
432 <http://www.sciencedirect.com/science/article/pii/S0896627315008235>, doi: 10.1016/j.neuron.2015.09.034.
- 433 **Gerstner W**, Kistler WM, Naud R, Paninski L. Neuronal dynamics: From single neurons to networks and models
434 of cognition. Cambridge University Press; 2014.
- 435 **Gregoriou GG**, Gotts SJ, Zhou H, Desimone R. High-Frequency, Long-Range Coupling Between Prefrontal and
436 Visual Cortex During Attention. *Science*. 2009 May; 324(5931):1207–1210. [http://science.sciencemag.org/
437 content/324/5931/1207](http://science.sciencemag.org/content/324/5931/1207), doi: 10.1126/science.1171402.
- 438 **Greicius MD**, Krasnow B, Reiss AL, Menon V. Functional connectivity in the resting brain: a network analysis of
439 the default mode hypothesis. *Proceedings of the National Academy of Sciences*. 2003; 100(1):253–258.

- 440 **Gross J**, Schmitz F, Schnitzler I, Kessler K, Shapiro K, Hommel B, Schnitzler A. Modulation of long-range neural
441 synchrony reflects temporal limitations of visual attention in humans. *Proceedings of the National Academy*
442 *of Sciences*. 2004; 101(35):13050–13055.
- 443 **Helfrich RF**, Schneider TR, Rach S, Trautmann-Lengsfeld SA, Engel AK, Herrmann CS. Entrainment of brain
444 oscillations by transcranial alternating current stimulation. *Current Biology*. 2014; 24(3):333–339.
- 445 **Jansen BH**, Rit VG. Electroencephalogram and visual evoked potential generation in a mathematical model of
446 coupled cortical columns. *Biological Cybernetics*. 1995; 73(4):357–366.
- 447 **König P**, Schillen TB. Stimulus-dependent assembly formation of oscillatory responses: I. Synchronization.
448 *Neural Computation*. 1991; 3(2):155–166.
- 449 **Li L**, Rilling JK, Preuss TM, Glasser MF, Damen FW, Hu X. Quantitative assessment of a framework for creating
450 anatomical brain networks via global tractography. *NeuroImage*. 2012; 61(4):1017–1030.
- 451 **Mantini D**, Perrucci MG, Del Gratta C, Romani GL, Corbetta M. Electrophysiological signatures of resting state
452 networks in the human brain. *Proceedings of the National Academy of Sciences*. 2007; 104(32):13170–13175.
- 453 **Messé A**, Rudrauf D, Giron A, Marrelec G. Predicting functional connectivity from structural connectivity via
454 computational models using MRI: an extensive comparison study. *NeuroImage*. 2015; 111:65–75.
- 455 **Raichle ME**. The brain's default mode network. *Annual Review of Neuroscience*. 2015; 38:433–447.
- 456 **Schmidt SL**, Iyengar AK, Foulser AA, Boyle MR, Fröhlich F. Endogenous cortical oscillations constrain neuromod-
457 ulation by weak electric fields. *Brain Stimulation*. 2014; 7(6):878–889.
- 458 **Siegel M**, Donner TH, Engel AK. Spectral fingerprints of large-scale neuronal interactions. *Nature Reviews*
459 *Neuroscience*. 2012; 13(2):121.
- 460 **Van Den Heuvel MP**, Pol HEH. Exploring the brain network: a review on resting-state fMRI functional connectivity.
461 *European Neuropsychopharmacology*. 2010; 20(8):519–534.
- 462 **Van Veen BD**, Van Drongelen W, Yuchtman M, Suzuki A. Localization of brain electrical activity via linearly
463 constrained minimum variance spatial filtering. *IEEE Transactions on Biomedical Engineering*. 1997; 44(9):867–
464 880.
- 465 **Wedeen VJ**, Wang R, Schmahmann JD, Benner T, Tseng WYI, Dai G, Pandya D, Hagmann P, D'Arceuil H,
466 de Crespigny AJ. Diffusion spectrum magnetic resonance imaging (DSI) tractography of crossing fibers.
467 *NeuroImage*. 2008; 41(4):1267–1277.
- 468 **Yazdan-Shahmorad A**, Silversmith DB, Kharazia V, Sabes PN. Targeted cortical reorganization using optogenetics
469 in non-human primates. *eLife*. 2018; 7:e31034.